

RAPID COMMUNICATIONS

Polarization-controlled and single-transverse-mode vertical-cavity surface-emitting lasers with eye-shaped oxide aperture

To cite this article: Jiye Zhang *et al* 2018 *Jpn. J. Appl. Phys.* **57** 120309

View the [article online](#) for updates and enhancements.



Polarization-controlled and single-transverse-mode vertical-cavity surface-emitting lasers with eye-shaped oxide aperture

Jiye Zhang^{1,2}, Jianwei Zhang^{1*}, Xing Zhang¹, Yongqiang Ning¹, Hongbo Zhu¹, Werner Hofmann³, Jun Zhang¹, Yugang Zeng¹, Youwen Huang¹, Lei Xiang^{1,2}, Yingying Liu^{1,2}, Li Qin¹, and Lijun Wang¹

¹State Key Laboratory of Luminescence and Applications, Changchun Institute of Optics, Fine Mechanics and Physics, Chinese Academy of Sciences, Changchun 130033, China

²University of Chinese Academy of Sciences, Beijing 100049, China

³Technical University of Berlin, Berlin 10623, Germany

*E-mail: zjw1985@ciomp.ac.cn

Received July 27, 2018; accepted September 23, 2018; published online October 31, 2018

We presented a single-transverse-mode and single-polarization vertical-cavity surface-emitting laser (VCSEL) with an eye-shaped oxide aperture, obtained by enhanced anisotropic oxidation of oxide layer. For apertures with dimensions of 2×4.6 and $3 \times 6 \mu\text{m}^2$, the orthogonal polarization suppression ratio (OPSR) of the VCSEL was 22 and 19 dB, respectively. A single-mode suppression ratio (SMSR) of more than 25 dB at an output power of 0.5 mW was also achieved for the VCSEL with aperture dimension of $2 \times 4.6 \mu\text{m}^2$. We believe that the proposed method to realize the mode and polarization control of VCSELs has great potential in future applications. © 2018 The Japan Society of Applied Physics

Vertical-cavity surface-emitting lasers (VCSELs) are the smallest and economically efficient laser emitters developed so far.^{1,2} The unique geometry of VCSELs results in several significant advantages over their edge-emitting counterparts, including low power consumption and longitudinal single-mode operation. However, unlike conventional edge emitting lasers, where the anisotropic structure geometry determines the output polarization in a natural way, cylindrically symmetric VCSELs are prone to unstable polarization.^{3,4} This is a crucial limiting factor for polarization-sensitive applications, such as optical communication, optical information processing, and atomic sensors.^{5,6} Thus, extensive attempts have been made to stabilize the polarization states of VCSELs, such as the use of fine metal-interlaced gratings, external optical feedback, electro-optic birefringence, photonic crystals, and high contrast grating structures.^{7–12} However, the large-scale fabrication of VCSELs with these complex processes is difficult to realize. An oriented GaAs substrate can introduce anisotropic optical gain in the active region of VCSELs, thus realizing polarization.^{13,14} Polarization control can also be achieved by using structurally anisotropic self-assembled quantum dots as active layers in VCSELs.^{15,16} The above studies employed excellent techniques in the field of crystal growth for VCSEL structures, but these techniques cannot be easily used by other researchers. A typical method to control the polarization direction of VCSELs is to fabricate anisotropic oxide apertures, and this has been demonstrated by fabricating a VCSEL array with a rectangular mesa structure.¹⁷ A method to introduce an asymmetric oxide aperture itself is of course another ideal solution. This has been practically achieved for red-emitting VCSELs,¹⁸ whose polarization stability is attributed to the effects of spontaneous ordering during metal–organic vapor phase epitaxy (MOVPE) growth of the GaInP material system, which leads to a reduction in crystal symmetry.¹⁹ The NIR-emitting VCSELs are normally polarization-unstable due to the crystal symmetry of AlGaAs materials. However, oxidation apertures with an asymmetric shape can also be obtained, because the anisotropy of lateral oxidation along different crystal directions can be controlled via the oxidation conditions.^{20,21} Additionally, the oxidation rate along different crystal directions can be affected by the

mechanical stress resulting from the volumic shrinkage that occurs during the oxidation, especially when the Al content of the oxide layer exceeds 98%.^{22,23} However, realizing the stable polarization control of VCSELs via the anisotropy of the oxidation process of AlGaAs compounds has been the subject of very few studies in spite of its high relevance to photonic device applications.

In this letter, we report on eye-shaped oxide apertures to enhance the polarization stability of VCSELs. First, we describe the structure of our VCSEL and explain the selection principle of key parameters. Secondly, the oxide apertures with a shuttle shape are presented and explained. Finally, the polarization characteristics of VCSELs with shuttle-shape apertures of different dimensions are shown. In this study, the single-mode and single-polarization operation of VCSELs is simultaneously achieved when the dimensions of the shuttle-shaped aperture are $2 \times 4.6 \mu\text{m}^2$. An orthogonal polarization suppression ratio (OPSR) of more than 21 dB and a single-mode suppression ratio (SMSR) of more than 25 dB at an output power of 0.5 mW are achieved.

A schematic diagram of the epitaxial structure of our VCSEL is shown in Fig. 1. The MOVPE-grown 890 nm VCSEL wafer was fabricated on an n-type GaAs(100) substrate. The carbon-doped p-type distributed Bragg reflector (DBR) in the VCSEL consisted of 22 pairs of $\text{Al}_{0.1}\text{Ga}_{0.9}\text{As}/\text{Al}_{0.9}\text{Ga}_{0.1}\text{As}$ layers. For selective oxidation, the oxide layer was partially used instead of the $\text{Al}_{0.9}\text{Ga}_{0.1}\text{As}$ layer, near the active region, in the p-side DBR. The AlAs material was used as the oxide layer because it shows more anisotropic oxidation during the oxidation process than the traditional $\text{Al}_{0.98}\text{Ga}_{0.02}\text{As}$. The thickness of the AlAs oxide layer was chosen as 70 nm, which was much thicker than the traditional oxide layer of 30 nm. Thus, the stress-induced difference in the oxidation rate along the orthogonal crystal directions is enhanced.²⁴ A circular mesa was defined using photolithography and inductively coupled plasma (ICP) to allow the lateral oxidation of the buried AlAs from its etched sidewall.

The samples were then oxidized at 410 °C in a saturated $\text{N}_2/\text{H}_2\text{O}$ mixture produced at 93 °C. To increase the anisotropy during the oxidation process, the gas distribution within the oxidation furnace was controlled. An exhaust pump was connected to the furnace chamber. The pumping rate was

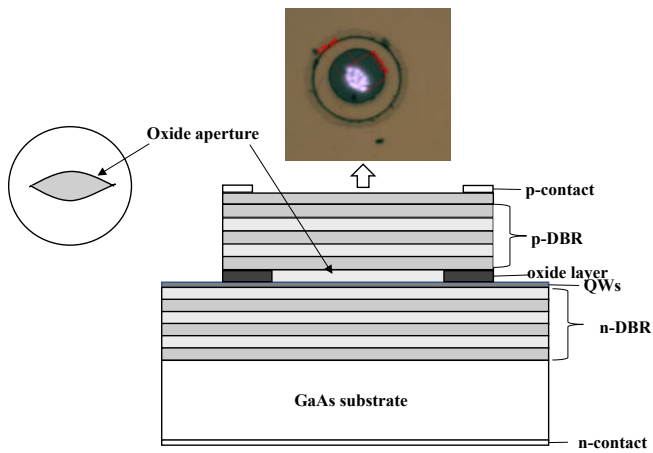


Fig. 1. (Color online) Schematic cross-sectional view of the VCSEL structure: the near field of the VCSEL with an eye-shaped oxide aperture is shown in the inserted figure.

slightly higher than the gas feed rate. Thus, an oriented flow direction of the moisture was formed within the chamber. During the oxidation process, the $\langle 110 \rangle$ crystal direction of the wafer was set perpendicular to the gas flow direction as the oxidation rate along this crystal direction is lower.²⁴⁾ Then lateral oxidation of the buried AIAs layer was carried out. A near-field top-view image of a final VCSEL device is shown as the inserted figure in Fig. 1. A shuttle-shaped emitting region can be clearly observed.

To describe the oxide aperture accurately, we etch the p-DBR of the oxidized sample away by H_2SO_4 and H_2O_2 solutions.²⁵⁾ Figures 2(a)–2(c) show top views of oxide apertures with different oxidation times. The mesa diameter is $30\ \mu\text{m}$ and the oxide apertures in the center of the mesa are a gray-white. The black region around the oxide aperture is the oxidized part of the AIAs layer, which is mostly Al_xO_y . Only a very small part of the oxidized layer still exists on the mesa because the outer part of the oxidized layer collapses beneath the p-DBR layers, which are laterally etched away by the chemical solutions. The gray-white region around the black region is not in the same plane as the black region, and it is formed from the residual p-DBR, the further etched active region, and the n-DBR. The etching rate of the InGaAs layers in the active region by our etching solutions is very low. Thus, the observed regions around the black layer are mainly the active region and the n-DBR region. As is known, the skirt effects around the bottom of a VCSEL mesa can be enhanced by a wet etching process. Thus, the size of the residual active region is larger than that of the original mesa structure. However, when the etching time is long enough, the p-DBR region can be laterally etched and become smaller. When the p-DBR layers outside the oxidized layers are etched away, only a very small part of the original mesa can be observed around the black oxidized layers, as shown in Fig. 2(b). During the above process, two circular gray-white areas can be observed due to the mask effect of the InGaAs layers within the active region, as shown in Figs. 2(a) and 2(c).

The shuttle-shape of the oxide apertures can be observed in Fig. 2. This shape means that anisotropy of the oxidation rate is realized during the AIAs oxidation process. The length along the short axis of the oxide aperture is defined as D_S and

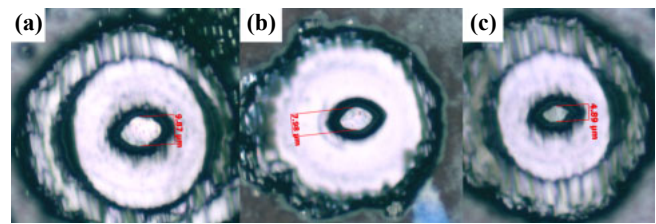


Fig. 2. (Color online) Oxide aperture of VCSEL samples with $30\ \mu\text{m}$ circular mesa and oxidation time are (a) 8 min, (b) 9 min, and (c) 10 min. The oxide aperture appears gray-white in the center of the mesa. The length of the oxide aperture along the short axis is identified.

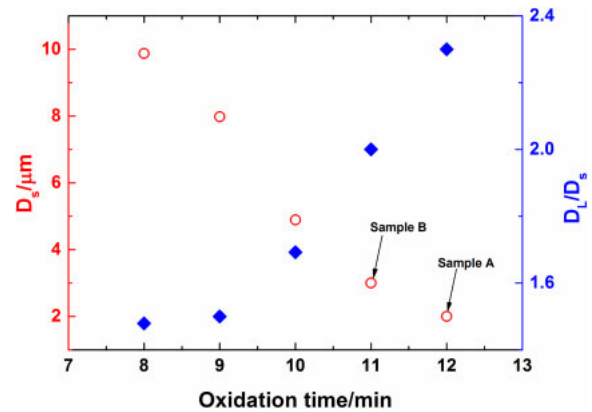


Fig. 3. (Color online) D_S and D_L/D_S dependences on the oxidation time. The red circles and blue diamonds represent D_S and D_L/D_S , respectively.

the length along the long axis is defined as D_L . As the oxidation time increases from 8 to 10 min, D_S decreases from 9.87 to $4.89\ \mu\text{m}$. Also, the oxidation rate of the AIAs layer along the short axis is about $1.25\ \mu\text{m}/\text{min}$. We can observe in Fig. 2 that D_L changes very slowly as the oxidation time increases. Thus, D_L/D_S is expected to increase when the oxidation time increases.

VCSEL samples with different oxidation time was fabricated and measured by the above method. The parameters D_S and D_L/D_S were obtained and are shown in Fig. 3. As the oxidation time increases, D_S first decreases rapidly then more slowly. This phenomenon is consistent with that reported in prior research on the isotropic oxidation of a circular mesa.¹⁷⁾ As the length along the long axis of the oxide aperture D_L changes much slower than D_S , D_L/D_S increases with increasing oxidation time. In fact, D_L/D_S increases rapidly when the oxidation time is longer than 10 min, as shown in Fig. 3. Thus, a narrower oxide aperture is expected for longer oxidation times. Oxide apertures with a narrower shape can realize more intense asymmetric confinement of the optical field and current within the active region of the VCSEL, and the stable polarization of the VCSEL can be expected. Following this principle, two samples were fabricated with oxidation time of 12 and 11 min, named samples A and B, respectively. D_S for samples A and B are 2 and $3\ \mu\text{m}$, as shown in Fig. 3. The ratios between D_L and D_S are 2.3 and 2 for samples A and B, respectively.

The polarization-resolved light–current (PRL–I) characteristics of samples A and B are shown in Fig. 4. The red and blue lines in Fig. 4 indicate the optical powers P_{0° and P_{90° measured behind a Glan–Thompson polarizer, respectively.

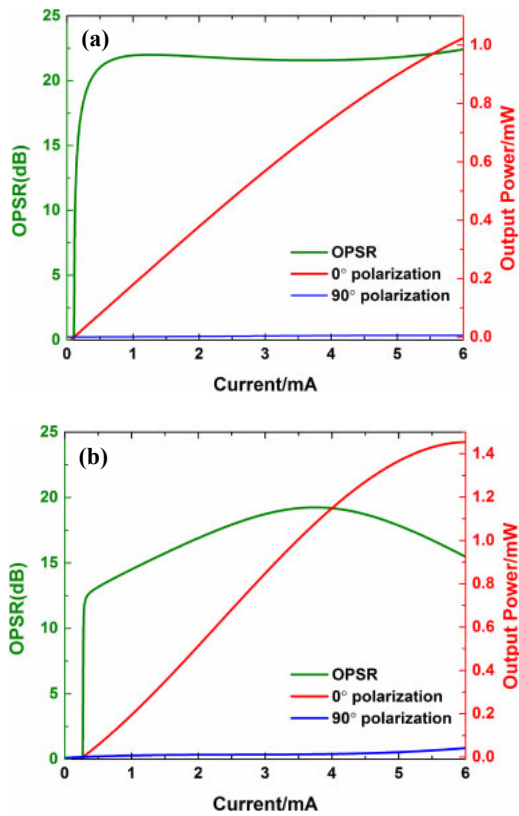


Fig. 4. (Color online) Polarization-resolved operation characteristics of samples A (a) and B (b). The red and blue lines represent the optical power along the long (0°) and short (90°) axes of the oxide aperture, respectively. The OPSR is defined as $OPSR = 10 \log(P_{0^\circ}/P_{90^\circ})$.

The optical transmission direction of the polarizer is parallel (0°) and orthogonal (90°) to the long axis of the oxide aperture, respectively, with no correction for the losses introduced by the polarizer. The threshold current of sample A is extremely low, as shown in Fig. 4(a) and a maximum magnitude of the OPSR of as high as 22 dB is obtained for sample A, where $OPSR = 10 \log(P_{0^\circ}/P_{90^\circ})$. Sample A shows very stable polarization up to thermal roll-over. The oxide aperture of sample B is larger than that of sample A. Thus, the threshold current of sample B is higher than that of sample A, as shown in Fig. 4(b). The maximum OPSR of sample B is about 19 dB and the OPSR of sample B at different operating currents is not as high as that of sample A. The main reason for this may be that D_L/D_S of sample B is lower than that of sample A, as shown in Fig. 3. The optical power orthogonal (90°) to the long axis of the oxide aperture increases when the operating current exceeds 4.5 mA in Fig. 4(b) and the optical power parallel (0°) to the long axis of the oxide aperture begins to roll over at this operating current. Thus, the OPSR of sample B decreases when the operating current exceeds 4.5 mA, as shown in Fig. 4(b). However, the polarization orientation of sample B is still very stable during the whole operating range, and the OPSR reaches 15 dB even at the thermal roll-over point. These results demonstrate that we have realized the stable polarization control of VCSELs even when their mesa is circular.

VCSELs with a single transverse mode and single polarization are very useful for numerous applications. The high-resolution lasing spectra of sample A operated at different currents were measured by a Yokogawa AQ6370D spectrom-

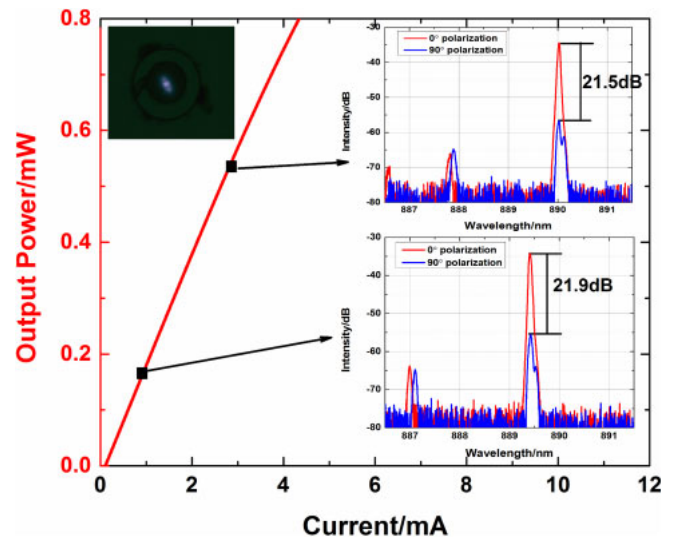


Fig. 5. (Color online) Emission spectra of sample A at the operating currents of 1 and 3 mA. The red and blue lines represent the optical spectra along the long (0°) and short (90°) axes of the oxide aperture, respectively.

eter. Figure 5 shows the spectra of sample A at different operating currents. The inserted figure shows the near field of sample A operated near the threshold current, captured under a microscope. Shuttle-shaped emitting spots can be observed clearly for sample A, which is in accord with the shape of its oxide aperture.

A red-shift of the center wavelength can be observed in the spectra in Fig. 5, mainly caused by the internal self-heating effect of the VCSEL. The red lines in the spectra confirm that the SMSR exceeds 25 dB up to 3 mA, and the VCSEL delivers a single-mode output power of more than 0.5 mW. For sample A, the dimensions of both the long and short axes of the oxide aperture satisfy the transmission condition for a single transverse mode.²⁶⁾ This is the main reason for the single-transverse-mode operation of sample A. The polarization resolved spectra clearly show that a stable OPSR of more than 21 dB is also obtained, as indicated in the spectra in Fig. 5. The stable polarization is mainly due to the high aspect ratio of the eye-shaped oxide aperture. Thus, a single transverse mode and single polarization are achieved for the VCSEL with the circular mesa structure.

The far-field profiles along different axes of the shuttle-shaped oxide aperture of sample A are shown in Fig. 6. The divergence angle along the long axis is about 12.4° (FWHM), while that along the short axis is about 6.9°. The different divergence angles along the two directions are mainly caused by the asymmetrical shape of the oxide aperture. Although the far-field profile is not symmetric, in contrast to that of regular VCSELs, a tailored intensity distribution can be realized by using micro lenses. Also the optical system can be simple. Actually, the freedom to realize a wide variety of intensity distributions using VCSELs with an asymmetrical far-field shape can be acquired with one or more lenses, as has been proved by Miller and co-workers.^{27,28)}

We reported the achievements of a single-polarization and single-transverse-mode VCSEL by introducing a eye-shaped oxide aperture. Eye-shaped oxide apertures with different dimensions and aspect ratios were realized by the enhanced anisotropic oxidation of the AIAs layer. We demonstrated the

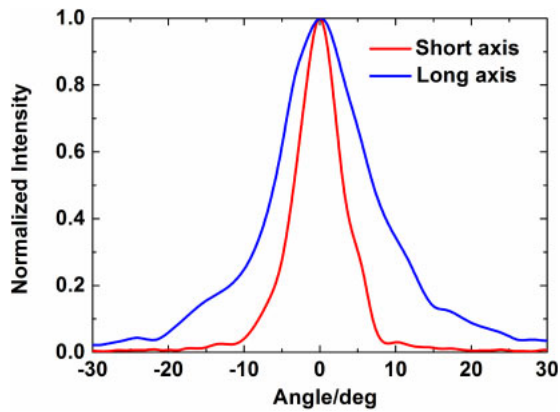


Fig. 6. (Color online) Far-field profile along each axis of the oxide aperture of sample A at a driving current of 3 mA.

single-mode and single-polarization operation for an oxide aperture with dimensions of $2 \times 4.6 \mu\text{m}^2$. An SMSR of more than 25 dB and an OPSR of more than 21 dB were achieved at an output power of more than 0.5 mW. For a larger oxide aperture with dimensions of $3 \times 6 \mu\text{m}^2$, the maximum OPSR of the VCSEL was 19 dB. Thus, we have reported a very feasible and effective method to realize the transverse mode and polarization control of VCSELs. We believe that this method can substantially reduce the cost of fabricating linearly polarized VCSELs and will be especially useful to control the polarization angle in large-scale VCSEL arrays.

Acknowledgments This work was supported by the National Key Research and Development Program of China (No. 2017YFB0503200); Fudan University–CIOMP Joint Fund (No. FC2017-002); The National Natural Science Foundation of China (Nos. 61434005, 11674314, 11774343, and 61727822); Chinese Academy of Sciences President’s International Fellowship Initiative (Grant No. 2018VTA0005); and Key Projects of Jilin Province Science and Technology Development Plan (Nos. 20180201119GX and 20160414016GH).

- 1) K. Iga, *IEEE J. Sel. Top. Quantum Electron.* **6**, 1201 (2000).
- 2) K. J. Ebeling, R. Michalzik, and H. Moench, *Jpn. J. Appl. Phys.* **57**, 08PA02 (2018).
- 3) A. Al-Samaneh, M. B. Sanayeh, S. Renz, D. Wahl, and R. Michalzik, *IEEE Photonics Technol. Lett.* **23**, 1049 (2011).
- 4) W. Wang, Y. Q. Ning, Z. H. Tian, X. Zhang, J. J. Shi, Z. F. Wang, L. S.

- Zhang, Y. Zhang, Y. Liu, L. Qin, and L. J. Wang, *Opt. Commun.* **284**, 1335 (2011).
- 5) S. Knappe, V. Shah, P. Schwindt, L. Hollberg, J. Kitching, L. A. Liew, and J. Moreland, *Appl. Phys. Lett.* **85**, 1460 (2004).
- 6) A. Al-Samaneh, M. B. Sanayeh, M. J. Miah, W. Schwarz, D. Wahl, A. Kern, and R. Michalzik, *Appl. Phys. Lett.* **101**, 171104 (2012).
- 7) S. J. Schablitsky, L. Zhuang, R. C. Shi, and S. Y. Chou, *Appl. Phys. Lett.* **69**, 7 (1996).
- 8) L. J. Sargent, J. M. Rorison, M. Kuball, R. V. Penty, I. H. White, S. W. Corzine, M. R. T. Tan, S. Y. Wang, and P. J. Heard, *Appl. Phys. Lett.* **76**, 400 (2000).
- 9) F. Rogister, D. Pieroux, M. Sciamanna, P. Megret, and M. Blondel, *Opt. Commun.* **207**, 295 (2002).
- 10) D.-S. Song, Y.-J. Lee, H.-W. Choi, and Y.-H. Lee, *Appl. Phys. Lett.* **82**, 3182 (2003).
- 11) M. C. Y. Huang, Y. Zhou, and C. J. Chang-Hasnain, *Nat. Photonics* **1**, 119 (2007).
- 12) T. Mukaiyama, N. Ohnoki, Y. Hayashi, N. Hatori, F. Koyama, and K. Iga, *IEEE J. Sel. Top. Quantum Electron.* **1**, 667 (1995).
- 13) M. Takahashi, P. O. Vaccaro, T. Watanabe, T. Mukaiyama, F. Koyama, and K. Iga, *Jpn. J. Appl. Phys.* **35**, 6102 (1996).
- 14) K. Tateno, Y. Ohiso, C. Amano, A. Wakatsuki, and T. Kurokawa, *Appl. Phys. Lett.* **70**, 3395 (1997).
- 15) H. Saito, K. Nishi, S. Sugou, and Y. Sugimoto, *Appl. Phys. Lett.* **71**, 590 (1997).
- 16) Y. Higuchi, S. Osaki, T. Kitada, S. Shimomura, Y. Takasuka, M. Ogura, and S. Hiyamizu, *Solid-State Electron.* **50**, 1137 (2006).
- 17) T. Yoshikawa, H. Kosaka, K. Kurihara, M. Kajita, Y. Sugimoto, and K. Kasahara, *Appl. Phys. Lett.* **66**, 908 (1995).
- 18) S. Weidenfeld, M. Eichfelder, M. Wiesner, W. M. Schulz, R. Rosbach, M. Jetter, and P. Michler, *IEEE J. Sel. Top. Quantum Electron.* **17**, 724 (2011).
- 19) S. Weidenfeld, H. Niederbracht, M. Eichfelder, M. Jetter, and P. Michler, *Proc. SPIE* **8432**, 843205 (2012).
- 20) G. Lafleur, G. Almuneau, A. Arnoult, H. Camon, and S. Calvez, *Opt. Mater. Express* **8**, 1788 (2018).
- 21) S. Calvez, G. Lafleur, A. Arnoult, A. Monmayrant, H. Camon, and G. Almuneau, *Opt. Mater. Express* **8**, 1762 (2018).
- 22) K. D. Choquette, K. M. Geib, C. I. H. Ashby, R. D. Twesten, D. Mathes, R. H. O. Blum, H. Q. Hou, D. M. Follstaedt, and B. E. Hammons, *IEEE J. Quantum Electron.* **3**, 916 (1997).
- 23) F. Chouchane, G. Almuneau, A. N. Cherkashin, A. Arnoult, G. Lacoste, and C. Fontaine, *Appl. Phys. Lett.* **105**, 041909 (2014).
- 24) P. O. Vaccaro, K. Koizumi, K. Fujita, and T. Ohachi, *Microelectron. J.* **30**, 387 (1999).
- 25) J. Zhang, Y. Ning, X. Zhang, Y. Zeng, J. Zhang, and L. Wang, *Opt. Laser Technol.* **56**, 343 (2014).
- 26) V. P. Kalosha, N. N. Ledentsov, and D. Bimberg, *Appl. Phys. Lett.* **101**, 071117 (2012).
- 27) S. Gronenborn, J. Pollmann-Retsch, P. Pekarski, M. Miller, M. Strösser, J. Kolb, H. Mönch, and P. Loosen, *Appl. Phys. B* **105**, 783 (2011).
- 28) H. Moench, S. Gronenborn, M. Miller, and P. Loosen, *Proc. SPIE* **7952**, 795207 (2011).